

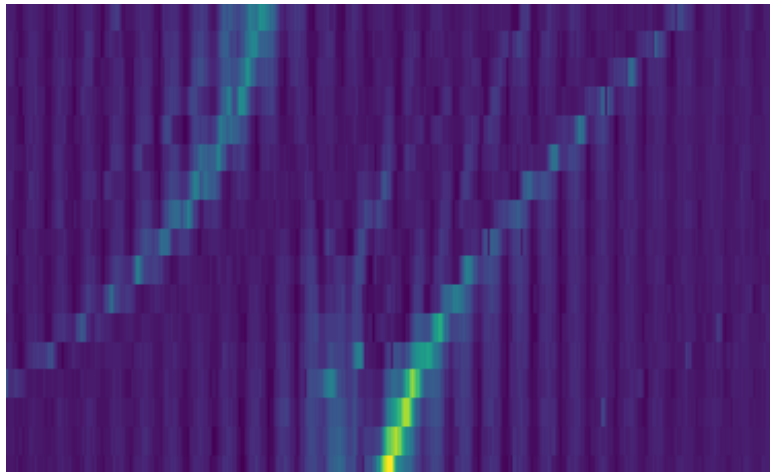
PRACTICAL COURSE III

# CIRCUIT QUANTUM ELECTRODYNAMICS

---

*Otto T.P. Schmidt*

November 13, 2021



## Abstract

Two-level quantum systems are the fundamental **feature** of quantum computing. However, the quantum states need to be controlled for any quantum computation.

This experiment introduces a possible realisation of such a controlled two-level regime, the circuit quantum electrodynamics (CQED). Instead of using an atom as quantum object, CQED establishes a two-level system by creating an artificial atom through electrical circuits.

In this construction two systems interact with each other, a cavity and the circuit (to which we will refer as qubit).

After an analysis of the cavity, we will inspect the interaction of the systems cavity and qubit and derive the coupling strength for a set of parameters.

# Contents

<b>1</b>	<b>Introduction</b>	<b>4</b>
<b>2</b>	<b>Quantum Information Theory</b>	<b>5</b>
2.1	Transmon . . . . .	5
2.1.1	Josephson Junction . . . . .	6
2.1.2	Tunability and SQUID loop . . . . .	7
2.2	Jaynes-Cummings model . . . . .	8
2.2.1	Dispersive and resonant regime . . . . .	9
2.2.2	Beyond a two-level approximation . . . . .	10
<b>3</b>	<b>Data analysis</b>	<b>11</b>
3.1	Cavity spectroscopy . . . . .	11
3.1.1	Observations . . . . .	12
3.1.2	Analysis . . . . .	13
3.1.3	Lorentzian fit . . . . .	14
3.2	Coil sweep . . . . .	17
3.2.1	Observations . . . . .	17
3.2.2	Analysis . . . . .	19
<b>4</b>	<b>Conclusion</b>	<b>25</b>
	<b>Appendices</b>	<b>26</b>
<b>A</b>	<b>Appendix A</b>	<b>26</b>
<b>B</b>	<b>Appendix B</b>	<b>26</b>

B.1	Shortest distance . . . . .	26
B.2	Avoided crossing . . . . .	28

# 1 Introduction

Quantum computing is all about controllability. We therefore need to understand the interaction of a 3D microwave cavity and a qubit. For this we need a measure of interaction of both systems, the coupling strength  $g$ .

In classic quantum electrodynamic (i.e. cavity QED), the coupling strength describes the atom-photon interaction. However, the stability and controllability of atoms is small compared to modern artificial atoms, namely superconducting two-level circuits. Therefore, for the system at hand, the coupling strength quantizes the interaction of the cavity and the superconducting qubit.

The first part of this experiment will consist in the analysis of the uncoupled cavity. The main goal is to determine the difference of the resonance frequency between the bare, uncoupled and the coupled cavity.

After the cavity is characterized we can proceed to the main part, the estimation of  $g$ . For different input powers of the signal we will tune the system with an external magnetic field and observe the transmitted frequencies. A suitable Hamiltonian for the two-level system will then introduce the coupling strength.

The following data analysis will illustrate and discuss the findings.

## 2 Quantum Information Theory

In theory, a quantum system should be able to control the qubit. The most basic notation of this quantum mechanical form of the bit is:

$$|\psi\rangle = \alpha |g\rangle + \beta |e\rangle \quad (1)$$

Here the states  $|g\rangle$  and  $|e\rangle$  represent a ground and excited state of the system and  $|\alpha|^2 + |\beta|^2 = 1$ .

This qubit is technically realised by a construction of various superconducting circuits including inductors, capacitors and a Josephson junction. The qubit is therefore an intricate system of different parts. In the particular set-up we use a transmon qubit (transmission line shunted plasma oscillation qubit) which is placed inside a 3D copper cavity. The function and mechanism of the important parts and their theory will be outlined in the following.

### 2.1 Transmon

In principle the transmon is based on a quantized harmonic oscillator, i.e. an oscillator with equidistant energy levels. Such an oscillator can be constructed by means of an LC-circuit. In classical electronic notation the Hamiltonian of this circuit is

$$H_{LC} = \frac{Q^2}{2C} + \frac{\Phi^2}{2L} \quad (2)$$

where  $Q$  is the charge on the capacitor,  $C$  the capacitance,  $\Phi$  the magnetic flux of the inductor and  $L$  the inductance.

Observables correspond to linear operators in quantum mechanics. If we follow the translation from the classic mechanical to quantum electronic Hamiltonian (see Appendix A), we can define the annihilation and creation operators

$$\begin{aligned} \hat{a} &= \frac{1}{\sqrt{2\hbar Z}}(Z * \hat{Q} + i\hat{\Phi}) \\ \hat{a}^\dagger &= \frac{1}{\sqrt{2\hbar Z}}(Z * \hat{Q} - i\hat{\Phi}) \end{aligned}$$

with the impedance  $Z = \sqrt{L/C}$  of the circuit.

With this the quantum electronic Hamiltonian of the LC-circuit reads

$$H = \hbar\omega(\hat{a}^\dagger\hat{a} + \frac{1}{2}) \quad (3)$$

This oscillator and its Hamiltonian define the fundamental quantum properties of the qubit. However, this system is only the basis for the transmon and needs to be adjusted.

### 2.1.1 Josephson Junction

Now that the Hamiltonian of the fundamental quantum system, the harmonic oscillator, has been established, the question of distinguishability of different states arises. The problem is that the energy spacing for the LC-circuit is equidistant. This makes it impossible to differentiate states. However, for the use in quantum computing precise tuning and identification of the eigenstates of the systems are necessary.

A regime with distinguishable eigenstates can be achieved if we introduce anharmonicity to the oscillator. This is possible with the implementation of a Josephson junction to the transmon. Figure 1 shows the difference between harmonic and anharmonic energy spacings.



Figure 1: Schematic of the harmonic and anharmonic oscillator energy states.[5]

The Josephson junction introduces the desired anharmonicity via the so called Josephson inductance

$$L_J = \frac{\Phi_0}{2\pi I_C} \frac{1}{\cos(\delta)} \quad (4)$$

where  $\Phi_0 = h/2e$ ,  $I_C$  is the critical current of the junction and  $\delta = \frac{2\pi\Phi(t)}{\Phi_0}$  with the magnetic flux  $\Phi(t)$ .

From the definition of the ladder operators  $\hat{a}^\dagger$ ,  $\hat{a}$  (with impedance  $Z = \sqrt{L_J/C}$ ) and equation 3 we can see the effect on the Hamiltonian of the LC, i.e. the shift of energies.

### 2.1.2 Tunability and SQUID loop

From the Josephson inductance we can see the dependence on an external ~~time-dependent~~ magnetic flux.

This external flux is captured by an additional part of the transmon, a SQUID (superconducting quantum interference device). With the SQUID the external magnetic flux is applied on the Josephson junction. This affects the qubit transition frequency  $\omega_q \approx 2\pi\sqrt{8E_C E_J(\Phi(t))}$  with  $E_C = 0.4$  GHz and  $E_J(\Phi) = E_{J,max}|\cos(\pi\Phi/\Phi_0)|$ . Here  $E_J$  is the Josephson energy and  $E_{J,max} = 53.5$  GHz.[2]

With this relation we can detune the cavities frequency and the qubits transition frequency. This results in a characteristic behaviour of the readout frequencies, which will be discussed in the following sections. Figure 2 shows this behaviour.

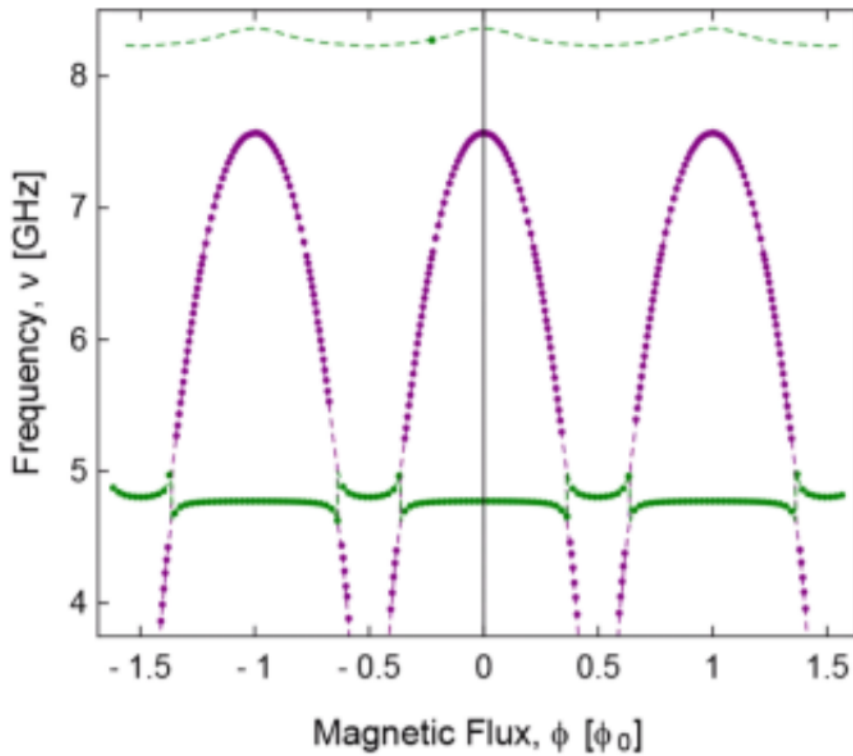



Figure 2: Characteristic development of the cavities readout energies/frequencies as a function of applied external magnetic flux  $\Phi$ . We can see the cosine oscillation described above. The qubits frequency is marked with purple dots, the cavities frequency with green dots.

## 2.2 Jaynes-Cummings model

The interaction of light with a two-level system, i.e. the transmon, and the resonant modes of the copper cavity is aptly described with the Jaynes-Cummings Hamiltonian. 

The operators of a two-level system can be depicted through Pauli matrices such that the qubit state Hamiltonian enters the model as

$$\hat{H}_Q = \frac{\hbar\omega_q}{2}\sigma^+\sigma^- = \frac{\hbar\omega_q}{2}\sigma_z \quad (5)$$

with  $\sigma^+ = |e\rangle\langle g|$  and  $\sigma^- = |g\rangle\langle e|$  the raising and lowering operators of the qubit (i.e.  $\sigma^+|g\rangle = |e\rangle$  and  $\sigma^-|e\rangle = |g\rangle$ ) and  $\omega_q$  the transition frequency of the qubit. The ground state has  $E = 0$ , the excited state  $E = \hbar\omega_q/2$ . The operators  $\hat{a}^\dagger$ ,  $\hat{a}$  of the basic LC-circuit are incorporated in these new operators.

The Hamiltonian of a cavity mode with frequency  $\omega_r$  is described by an harmonic oscillator

$$\hat{H}_C = \hbar\omega_r\hat{a}^\dagger\hat{a} \quad (6)$$

Therefore the energy eigenvalues of the cavity are  $E_C = \hbar\omega_r n$  with  $n$  the number of photons in the cavity.


The Jaynes-Cummings Hamiltonian captures the interaction of cavity and qubit with an additional coupling term. This coupling Hamiltonian reads

$$\hat{H}_I = \hbar g(\hat{a}\sigma^+ + \hat{a}^\dagger\sigma^-) \quad (7)$$

The two terms formulate the two interaction types of cavity and qubit. The first term  $\hat{a}\sigma^+$  refers to the annihilation of a photon and simultaneous excitation of the qubit whereas  $\hat{a}^\dagger\sigma^-$  describes the relaxation of the qubit into the ground state and creation of a photon. These interactions are weighted with the coupling strength  $g$ .

Combining the three parts we obtain the full Jaynes-Cummings Hamiltonian:

$$\hat{H}_{JC} = \hbar\omega_r\hat{a}^\dagger\hat{a} + \frac{\hbar\omega_q}{2}\sigma^+\sigma^- + \hbar g(\hat{a}\sigma^+ + \hat{a}^\dagger\sigma^-) \quad (8)$$

For the general product states  $|n, g\rangle$  and  $|n-1, e\rangle$  of the coupled system, we can formulate the matrix representation of the Jaynes-Cummings Hamiltonian 

$$\hat{H}_{JC} = \begin{pmatrix} \hbar\omega_r n & \hbar g\sqrt{n} \\ \hbar g\sqrt{n} & \hbar(n\omega_r + \omega_q) \end{pmatrix} \quad (9)$$



The eigenstates of this Hamiltonian are called dressed states and read [3]

$$\begin{aligned} |n, +\rangle &= \sin(\theta_n/2) |n, g\rangle + \cos(\theta_n/2) |n-1, e\rangle \\ |n, -\rangle &= \cos(\theta_n/2) |n, g\rangle - \sin(\theta_n/2) |n-1, e\rangle \end{aligned}$$

with  $\theta_n$  from  $\tan(\theta_n) = 2g\sqrt{n}/\Delta$  and eigenenergies

$$E_{\pm, n} = \hbar\omega_r n \pm \frac{\hbar}{2} \sqrt{4g^2 n + \Delta^2} \quad (10)$$

Here  $\Delta = \omega_r - \omega_q$  denotes the detuning of the system.

In this set-up we assume the strong coupling condition which assumes that  $\gamma, \kappa \ll g$  (with  $\gamma$  the atomic decay rate and  $\kappa$  the cavity decay rate). This means that the atomic system can absorb and re-emit a given photon many times before it leaks from the cavity or is spontaneously emitted. In this regime the Jaynes-Cummings model is fully realized.

The schematic of interaction between cavity and qubit is illustrated in figure 3.

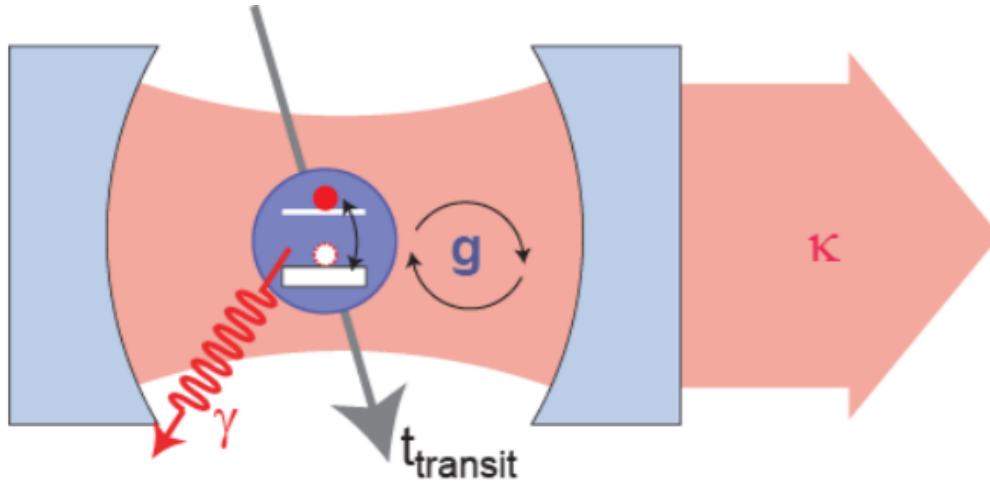


Figure 3: Schematic photon-qubit interaction with cavity decay rate  $\kappa$  and qubit decay rate  $\gamma$ . [3]

### 2.2.1 Dispersive and resonant regime

In the analysis of possible quantum states of the combined system we need to distinguish between the case where  $\Delta \approx 0$  and where  $g/\Delta \ll 1$ . The first case is called the resonant regime, the second dispersive.

The above defined Jaynes-Cummings Hamiltonian describes the eigenenergies (of frequencies) in the resonant regime.

Both regimes differ in the eigenenergies. For the resonant regime we have:

$$\Delta E = E_{+, n} - E_{-, n} = 2\hbar g \sqrt{n} \quad (11)$$

The anti-crossing of frequencies which will be discussed in section 3.2 is therefore an effect occurring in the resonant regime.

A schematic of the energy levels for a two-level qubit is shown below.

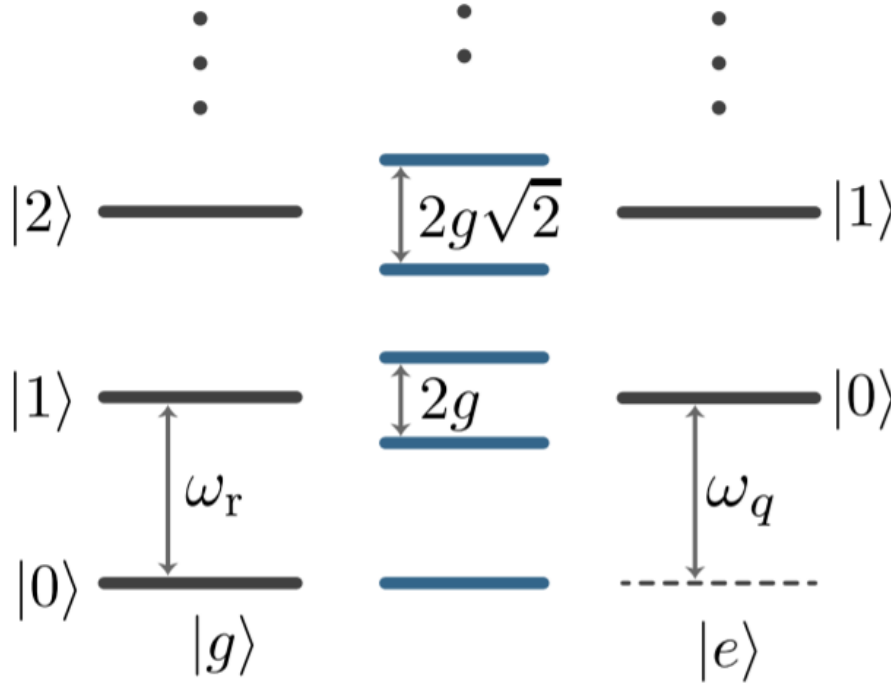


Figure 4: Energy spectrum of the Jaynes-Cummings Hamiltonian for uncoupled (grey) and coupled (blue) qubit-cavity system. The number of photons is given with  $|n = 0, 1, 2, \dots\rangle$ . [1]

In the dispersive regime the Hamiltonian changes. Since all measurements were taken in the avoided crossing region of the system, the dispersive regime and its Hamiltonian will not be outlined. A discussion of both the resonant and dispersive regime is given in [1].

### 2.2.2 Beyond a two-level approximation

For now only two states of the transmon are considered. However, to fully understand the interaction it may be necessary to introduce higher excitations of both the transmon and cavity.

### 3 Data analysis

Throughout the experiment the experimental set-up was not changed. The transmon and other technical parts in the wet fridge remained the same for all measurements.



However, for the different experimental runs different parameter sweeps and resolutions have been used.

All measurement were made on the Kelvinox set-up. In total two different experiments were conducted:

1. Cavity spectroscopy: in order to obtain the characteristics of the coupled system as well as the uncoupled cavity, a frequency sweep was made for a fixed external voltage.
2. Coil sweep: since the qubits transition frequency changes like the square of a cosine in time (see section 2.1.2), we can use a sweep in input frequency and coil voltage (results in magnetic flux) to observe how the readout energy of the cavity field changes. We will conduct a series of these two dimensional sweeps with different input power and analyse the result to obtain an estimate for the coupling strength  $g$ .

#### 3.1 Cavity spectroscopy

For this analysis the coil voltage was set to 0 V. At this constant voltage the qubits transition frequency should not change (see section 2.1.2). However, the amplitude of the input signal was changed. From equation 6 we can see how the amount of photons inside the cavity changes the energy of the coupled system.

The conversion from signal amplitude to dezibel (dB) is:

Amplitude ( $x$ ) to voltage ( $V$ ):

$$V(x) = A * \left( \frac{4x10^3}{0.15} \right) * C \quad (12)$$

with  $A = 1$  the input wave parameter and  $C = 1.5 \text{ V}$  the output range.

Voltage ( $v$ ) to dezibel ( $D$ ):

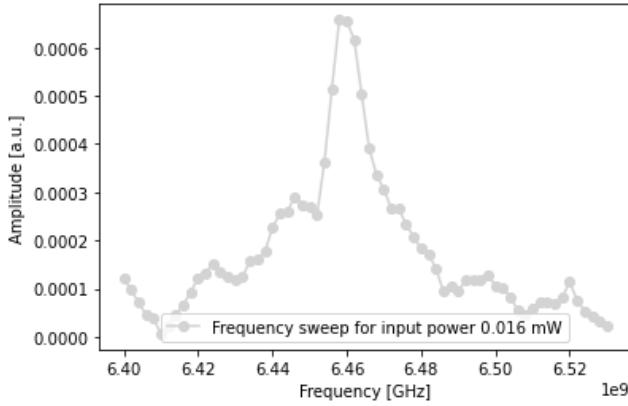
$$D(v) = 10 * \log_{10} \left( \frac{\left( \frac{v}{\sqrt{2}} \right)^2}{5 * 10^4} \right) \quad (13)$$

With this we can obtain the power of the signal in Watt ( $W$ ):

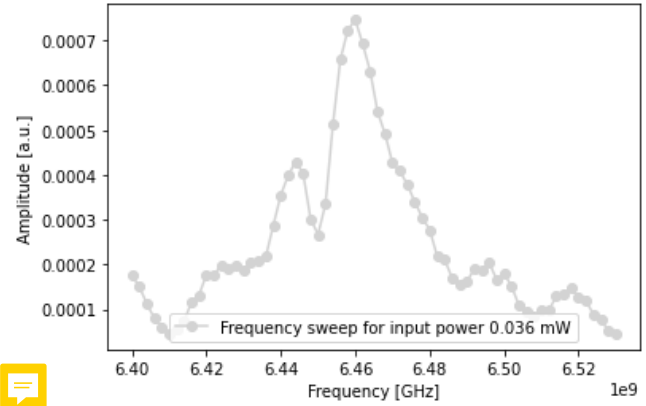
$$W(D) = 10^{\frac{dBm-30}{10}} \quad (14)$$

### 3.1.1 Observations

A series of frequency sweeps from 6.4 GHz to 6.53 GHz at coil voltage  $V = 0$  was conducted for various input amplitudes. The sampling frequency was 1.75 MHz. For each step the average from 10000 measurement was taken. These observations are shown in the succeeding graphs.

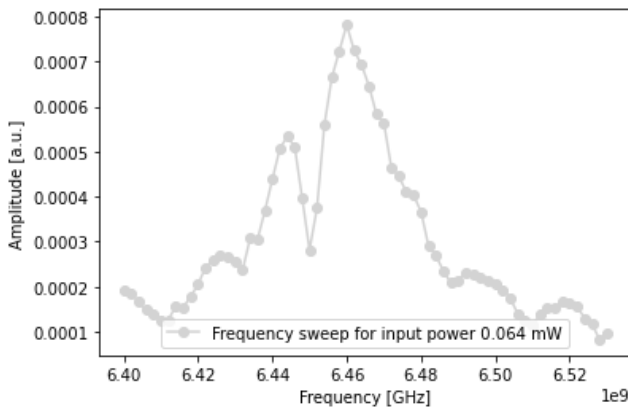


(a) Frequency sweep for 16.03  $\mu\text{W}$

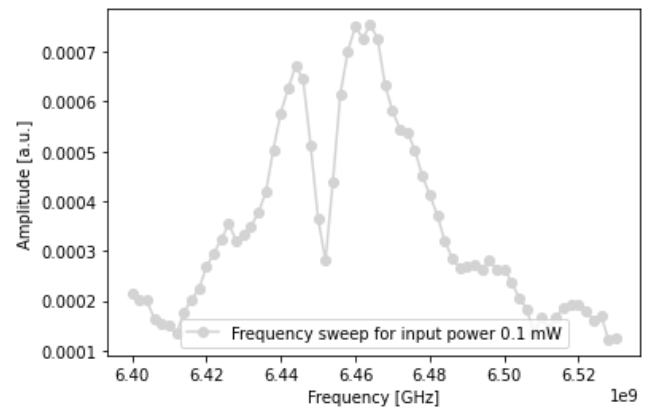


(b) Frequency sweep for 36.3  $\mu\text{W}$

Figure 5: Cavity spectroscopy for input amplitude  $\pm 2$  or 16.03  $\mu\text{W}$  and  $\pm 3$  or 36.3  $\mu\text{W}$ . The x-axis shows the frequency in GHz, the y-axis the amplitude in a.u.



(a) Frequency sweep for 64.12  $\mu\text{W}$



(b) Frequency sweep for 100  $\mu\text{W}$

Figure 6: Cavity spectroscopy for input amplitude  $\pm 4$  or 64.12  $\mu\text{W}$  and  $\pm 5$  or 100  $\mu\text{W}$ . The x-axis shows the frequency in GHz, the y-axis the amplitude in a.u.

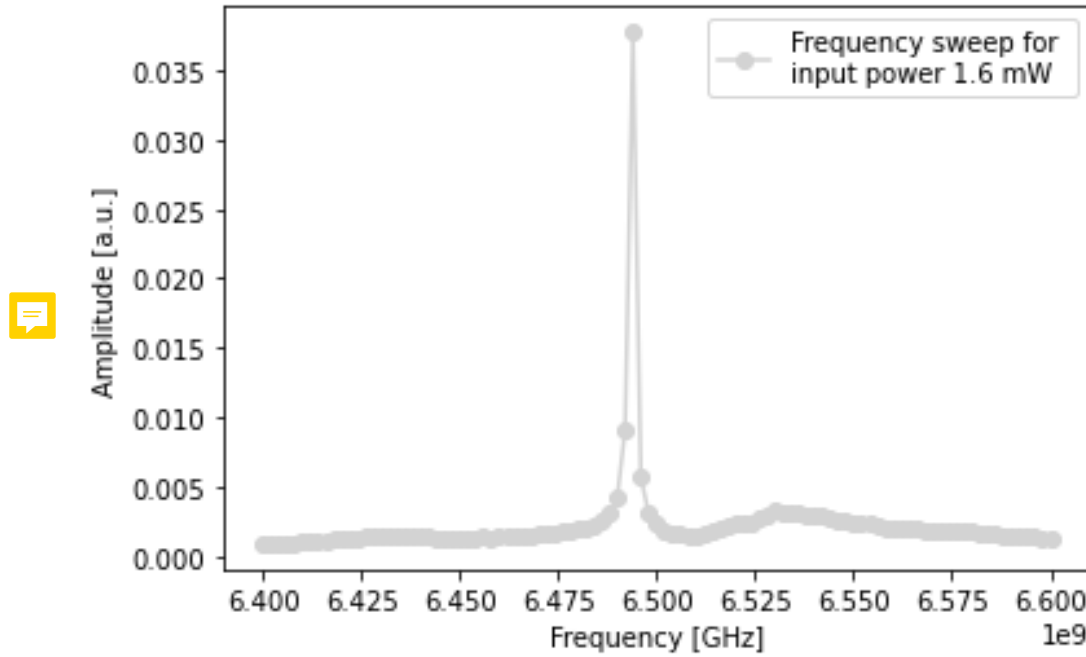


Figure 7: Cavity spectroscopy for input amplitude  $\pm 20$  or 1.6 mW. The x-axis shows the frequency in GHz, the y-axis the amplitude in a.u. Note that in this graph the frequency sweep is broader ( $\nu \in [6.4, 6.6]$  GHz) than in the graphs before.

### 3.1.2 Analysis

The presented observations bear some insights into the coupled system. Although no voltage is applied, the qubit still affects the readout frequency since the observations show not only the cavity but some additional interaction. The illustration 3 shows how cavity and qubit interact in general. Figure 3 therefore suggests a multi-modality in the avoided crossing region.

Before an analysis of the observations can be conducted, the regime of the system has to be known. The distinction between resonant and dispersive regime has been made in section 2.2.1. For the value  $V = 0$  cavity and qubit seem to be in the resonant regime (see section 3.2). With this assumption the observations can be properly analysed.

The graphs 5a, 5b, 6a and 6b show cavity-qubit interaction. In the resonant regime there seems to exist a second resonance frequency which increases for higher input power. This becomes visible if we fit graph 6b (where the multi-modality is most distinct) to a multi Lorentzian (see fig. 9 and section 3.1.3): a left peak, centered around  $\nu = 6.442$  GHz, and a right, primary peak at  $\nu = 6.464$  GHz are well pronounced.

However, when operated with very high input power, the multi-modality disappears and a sharp Lorentzian peak is visible (see figure 7). We also see that the fitted peak in figure 8 is centered

at  $\nu = 6.493$  GHz whereas the primary peak in figure 9 is centered around  $\nu = 6.464$  GHz.

The high input power seems to saturate the influence of the qubit on the readout frequency of the cavity. Therefore figure 7 shows the uncoupled cavity and  $\nu = 6.493$  GHz is the uncoupled cavity frequency.

For a high number of photons, the cavity term in the Jaynes-Cummings Hamiltonian dominates the interaction which is  $\propto g$ . Therefore the higher energy states of the harmonic oscillator crowd out the influence of the qubit.

### 3.1.3 Lorentzian fit

In order to properly identify possible resonant frequencies the fit to a Lorentzian is necessary. The single Lorentzian fit function reads:

$$f(\nu) = \frac{A\sigma^2}{((\nu - \nu_0)^2 + \sigma^2)} + C \quad (15)$$

Here  $A$  is an amplitude,  $\nu_0$  the center frequency,  $\sigma$  the width of the peak and  $C$  an axis shift.

The data set for figure 6b was fitted this simple Lorentzian.

The obtained parameters are given below in table 1.

Table 1: Values and standard deviations for the fitting parameters  $\nu_0$  and  $\sigma$  for the function  $f(\nu)$  in equation 15

$\nu_0$ [Hz]	$\sigma$ [Hz]
$(6.493 \times 10^9 \pm 7.803 \times 10^4)$	$(7.589 \times 10^5 \pm 7.518 \times 10^4)$

Similarly the fitting function for a twofold Lorentzian reads:

$$f(\nu) = \frac{A_1\sigma_1^2}{((\nu - \nu_{0,1})^2 + \sigma_1^2)} + \frac{A_2\sigma_2^2}{((\nu - \nu_{0,2})^2 + \sigma_2^2)} \quad (16)$$

Here again  $A_i$  is an amplitude,  $\nu_{0,i}$  the center frequency and  $\sigma_i$  the width of the peak with  $i$  the index of the  $i$ -th peak. The left peak with index  $i = 1$ , the right one with  $i = 2$ .

Table 2 shows the parameters and errors.

Table 2: Values and standard deviations for the fitting parameters  $A_i$ ,  $\nu_{0,i}$  and  $\sigma_i$  for the function  $f(\nu)$  in equation 16 for the open tube.

$A_1$ [a.u.]	$\nu_{0,1}$ [Hz]	$\sigma_1$ [Hz]
$(3.340 \times 10^{-4} \pm 4.609 \times 10^{-5})$	$(6.442 \times 10^9 \pm 5.321 \times 10^5)$	$(4.214 \times 10^6 \pm 1.060 \times 10^6)$
$A_2$ [a.u.]	$\nu_{0,2}$ [Hz]	$\sigma_2$ [Hz]
$(4.507 \times 10^{-4} \pm 5.700 \times 10^{-5})$	$(6.464 \times 10^9 \pm 5.839 \times 10^5)$	$(8.413 \times 10^6 \pm 1.658 \times 10^6)$

The corresponding fitted functions are plotted in figures 8 and 9.

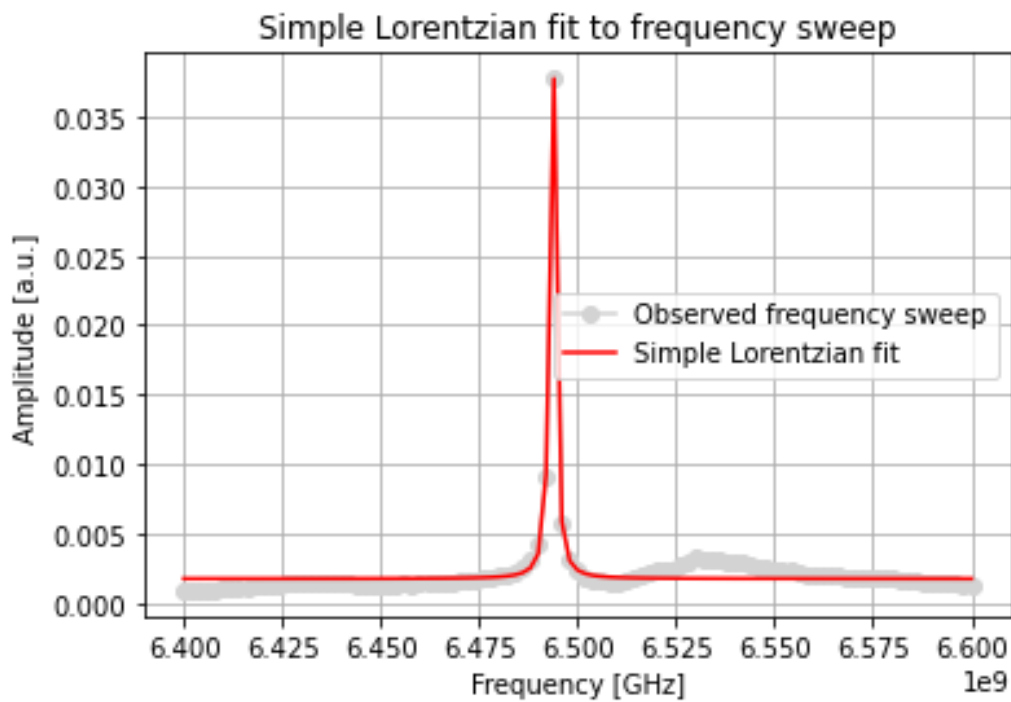


Figure 8: Fit to a simple Lorentzian. The corresponding data is plotted in grey and additionally in fig. 6b.

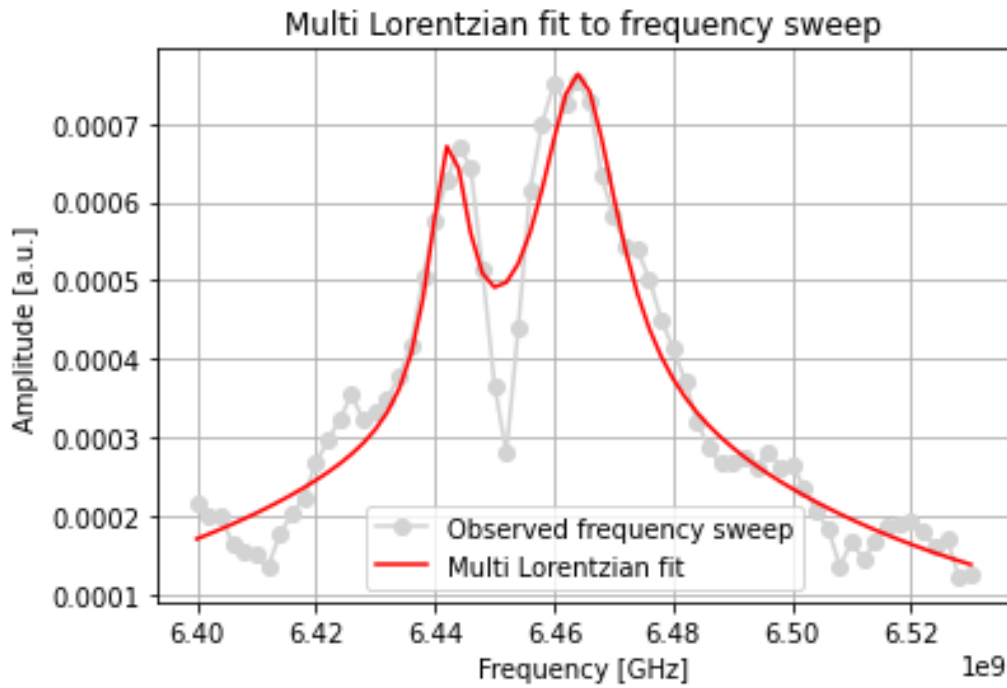


Figure 9: Fit to a multi Lorentzian. The corresponding data is plotted in grey and additionally in fig. 7.



## 3.2 Coil sweep

The analysis of the resonance frequencies for a certain coil voltage only gives a limited understanding of the cavity-qubit interaction. From section 2.1.2 we understand that the applied external voltage leads to a shift in the qubits resonance frequency.

A sweep through frequency and coil voltages would therefore also show the cavity-qubit system in different regimes (resonant and dispersive).

Figure 10 resembles the theoretical prediction illustrated in fig. 3 and shows how the interaction regimes recur periodically due to the  $\cos^2$  behaviour of the qubits frequency on external voltage.

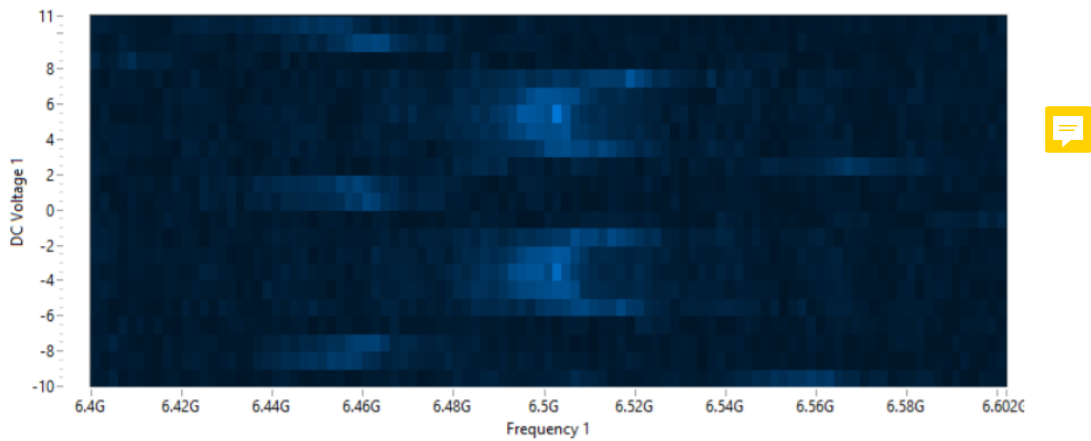


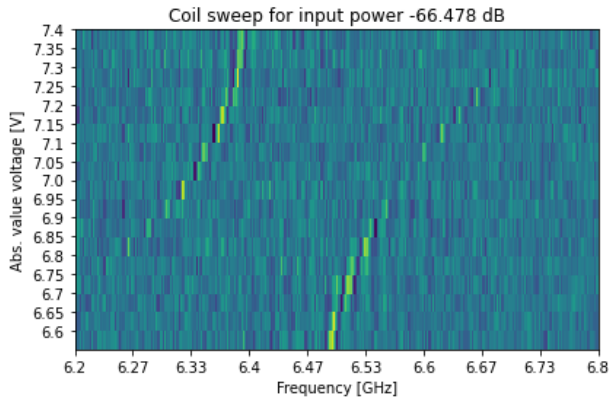
Figure 10: Two dimensional sweep for voltages. The x-axis shows the frequency sweep  $\nu \in [6.4, 6.6]$  GHz and the y-axis the voltage sweep  $V \in [-10, 10]$  V.

The goal of this experiment will be to obtain an estimate for the coupling strength  $g$ . This can be done if we analyse the resonant regime or equivalently the avoided crossing region in the coil sweep.

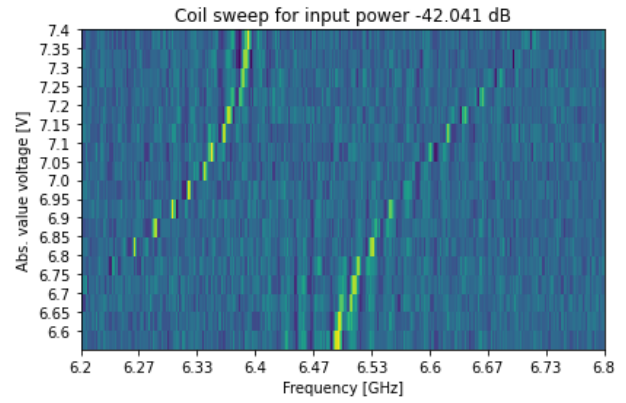
### 3.2.1 Observations

To obtain useful data for the avoided crossing region, the voltage interval was chosen to be  $V \in [-7.4, -6.6]$  V in steps of 50 mV. The frequency sweep was conducted for frequencies  $\nu \in [6.4, 6.6]$  GHz in steps of 2 MHz.

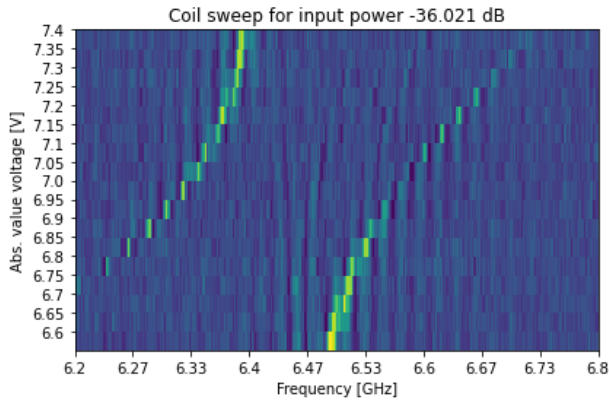
The raw data of the Kelvinox readout software *LabView* was imported and digitized with Python. The results are displayed for increasing input power below.



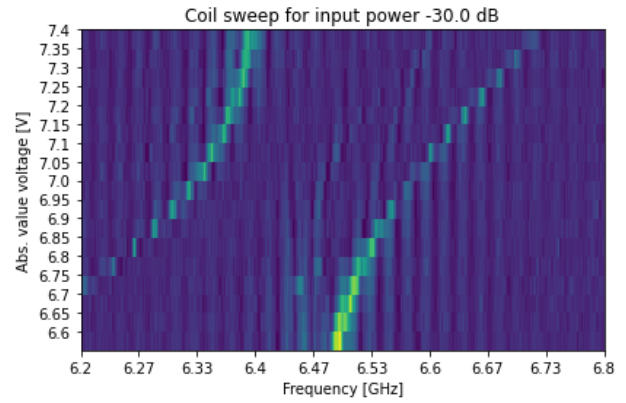
(a) Coil sweep for input power  $-66.478$  dB



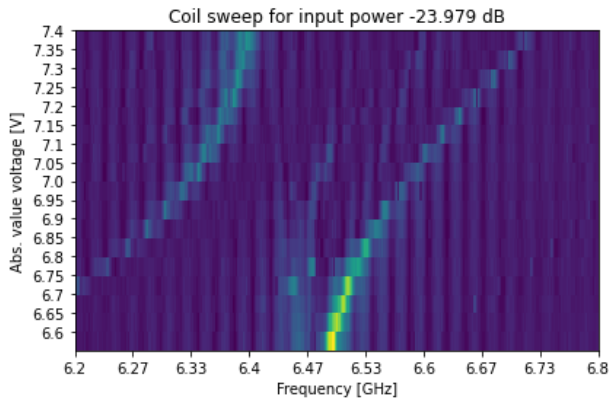
(b) Coil sweep for input power  $-42.041$  dB



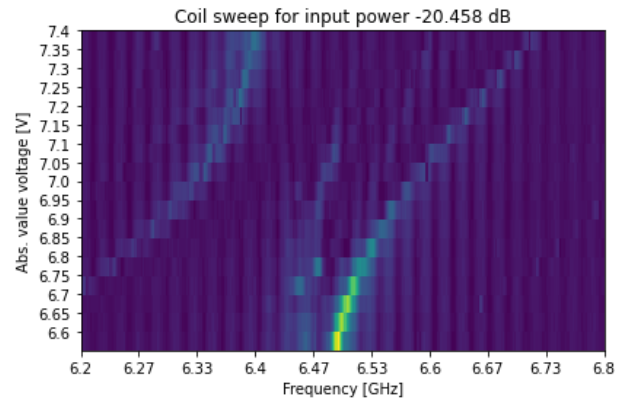
(c) Coil sweep for input power  $-36.021$  dB



(d) Coil sweep for input power  $-30$  dB



(e) Coil sweep for input power  $-23.979$  dB



(f) Coil sweep for input power  $-20.458$  dB

Figure 11: Two-dimensional frequency-voltage sweep for different input powers.

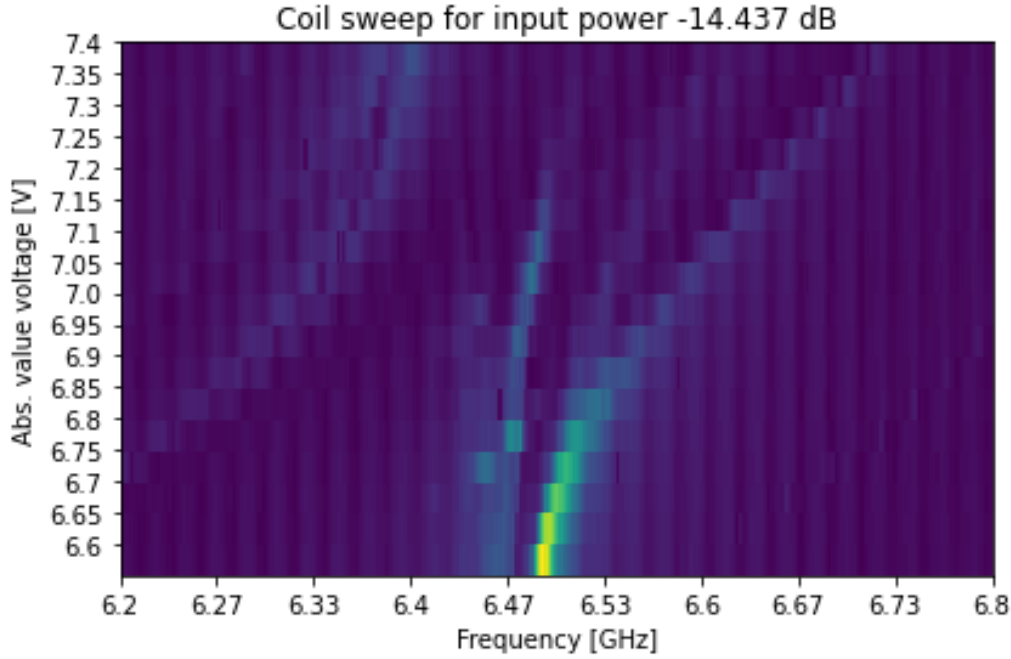


Figure 12: Coil sweep for input power  $-14.437$  dB

### 3.2.2 Analysis

The observations all show the behaviour of two cavity transmission branches. In order to calculate the coupling strength  $g$ , a mathematical understanding and modelling of the avoided crossing region has to be established.

In section 2.2 the eigenenergies of the Jaynes-Cummings Hamiltonian have been defined (see equation 10). Assuming that the avoided crossing takes place in the resonant regime (i.e.  $\Delta = 0$ ), the two branches become:

$$E_{+,n} = \hbar\omega_r n + \frac{\hbar}{2}\sqrt{4g^2n}$$

$$E_{-,n} = \hbar\omega_r n - \frac{\hbar}{2}\sqrt{4g^2n}$$

Hence we have an energy spacing of

$$\Delta E = 2g\hbar\sqrt{n} \quad (17)$$

which is equivalent to a minimal frequency spacing of

$$\Delta\nu \approx 2g \quad (18)$$



## Graphical analysis

With this approximation a preliminary graphical analysis of the data can be made. Since the two frequency branches correspond to a spacing of  $2g$  a graphical estimate for  $g$  can be determined which in turn can be used as fitting guesses for an analytical fit.

For that a function `shortest_dist` (see Appendix B.1) was written that extracts the intensity peaks of the two frequency branches and returns their position and an estimate for  $g$ , namely the shortest distance between all pairs.

The extracted peaks of figure 11a for instance are plotted in figure 13 below.

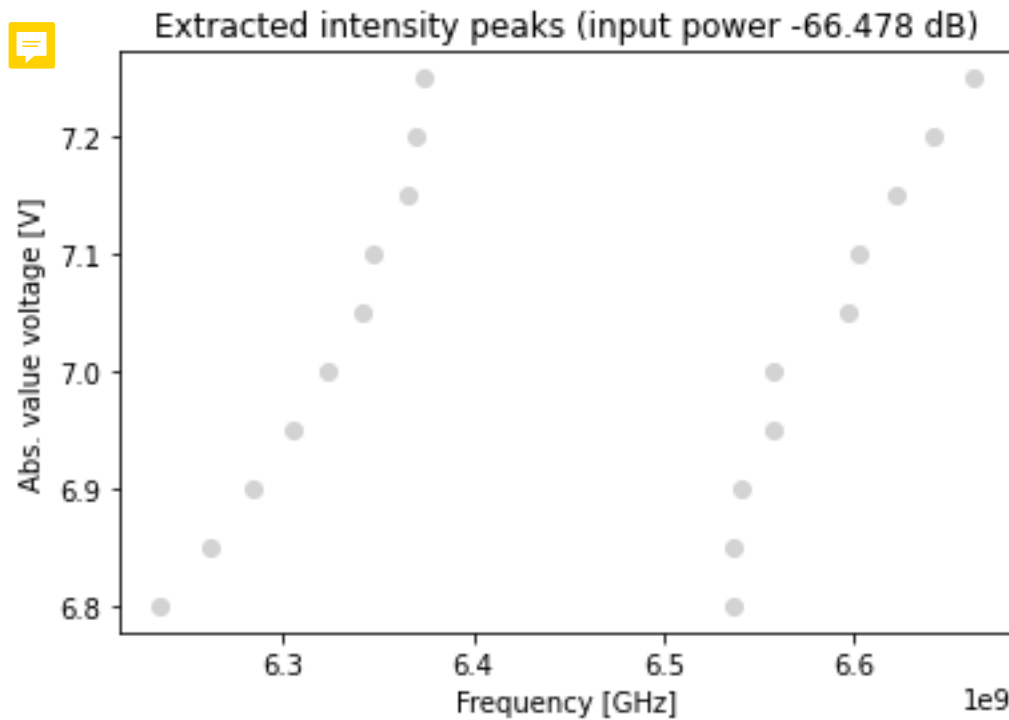


Figure 13: Extracted intensity peaks for the coil sweep for input power  $-66.478$  dB. Note that the voltage are gives in absolute values.

It is important to note that not the whole voltage interval is considered for the analysis. For voltages higher than  $-6.8$  V the noise near the uncoupled cavity resonance frequency ( $\nu = 6.493$  GHz) is very high. The distance between the two branches for these voltages is also never minimal. Therefore only the voltages with absolute value above  $6.8$  V are considered.

The graphical estimates for  $g$  are listed below.

Table 3: Graphical estimates for the coupling strength  $g$  for different input power. An error was attributed to the distance measurement since the frequency spacing is not infinitely fine and therefore gives room for ambiguity.

Input power [dB]	$g$ [GHz]
-66.478	$(0.117 \pm 0.001)$
-42.041	$(0.12 \pm 0.001)$
-36.020	$(0.121 \pm 0.001)$
-30.0	$(0.124 \pm 0.001)$
-23.979	$(0.126 \pm 0.001)$
-20.457	$(0.124 \pm 0.001)$
-14.436	$(0.125 \pm 0.001)$

These results can be plotted and fitted to analyse possible trends. This is shown in fig. 14.

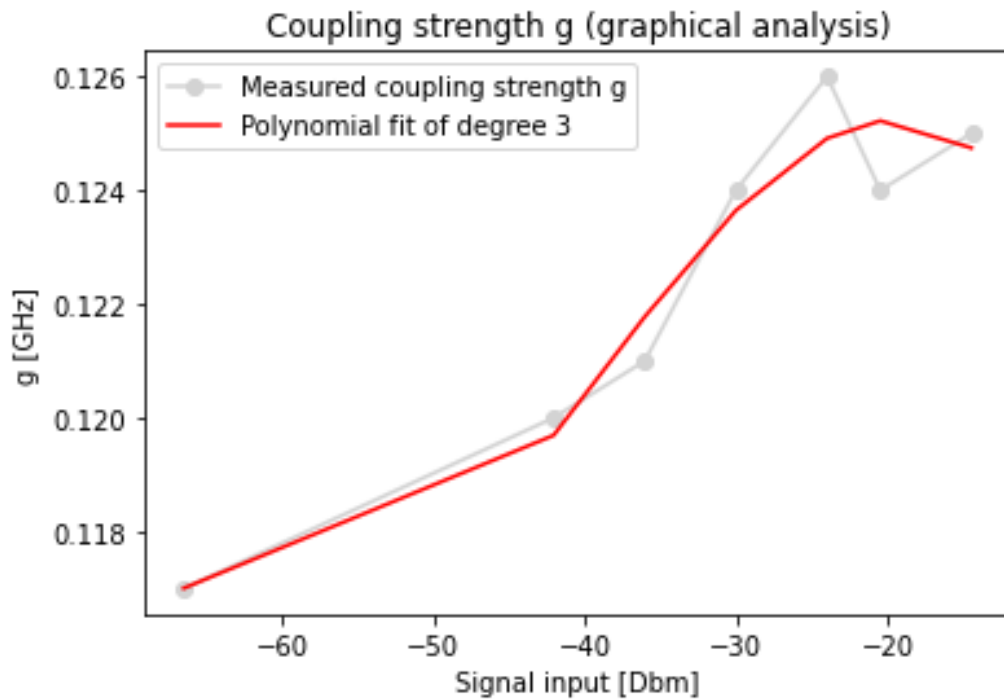


Figure 14: Plotted relation of table 3. A polynomial fit of degree 3 is also included to show a possible causal relation of input power to  $g$ .

## Mathematical analysis

The graphical analysis however remains a crude estimation for  $g$  since we only know  $\Delta\nu \approx 2g$ . A more subtle analysis of the avoided crossing and energy splitting can be made by considering the interaction Hamiltonian for the two-level system.

Let's consider the following simple model: a two-level system with zeroth-order states  $|\psi_a\rangle$  (with eigenfrequency  $f_a$ ) and  $|\psi_b\rangle$  (with eigenfrequency  $f_b$ ). The zeroth-order, uncoupled Hamiltonian then reads [4]:

$$\hat{H}_0 = |\psi_a\rangle f_a \langle\psi_a| + |\psi_b\rangle f_b \langle\psi_b| \quad (19)$$

Additionally we can construct a coupling Hamiltonian:

$$\hat{V} = |\psi_a\rangle g \langle\psi_b| + |\psi_b\rangle g \langle\psi_a| \quad (20)$$

We therefore get the full Hamiltonian:

$$\hat{H} = \begin{pmatrix} f_a & g \\ g & f_b \end{pmatrix} \quad (21)$$

Now we can make an assumption as to how the frequencies of the two states depend on the external voltage  $\Phi$ . We assume a linear dependence and have:

$$\begin{aligned} f_a &= \Phi c_a + f_{a,0} \\ f_b &= \Phi c_b + f_{b,0} \end{aligned}$$

Here  $c_i$  is some constant and  $f_{i,0}$  the center frequency. In this case,  $f_{i,0}$  corresponds to the mean frequency of each frequency branch.

The function `avoided_crossing_direct_coupling` incorporates the above theory (see Appendix B.2)

The eigenfrequencies (i.e. eigenvalues) of  $\hat{H}$  are the frequencies

$$f_{\pm} = \frac{f_a + f_b}{2} \pm \sqrt{\left(\frac{f_a - f_b}{2}\right)^2 + g^2} \quad (22)$$

Now that we understand the model underlying the function `avoided_crossing_direct_coupling`, we can use it as a fitting function. The coupling strength  $g$  and its standard deviation for the different input powers are displayed in table 4. As an example, the fitted frequency branches for input power  $-23.979$  dB are plotted in figure 15.

Table 4: Fitted parameters  $g$  and corresponding standard deviations for different input power.

Input power [dB]	$g$ [GHz]
-66.478	$(0.122 \pm 0.0018)$
-42.041	$(0.122 \pm 0.0012)$
-36.020	$(0.122 \pm 0.0011)$
-30.0	$(0.123 \pm 0.002)$
-23.979	$(0.125 \pm 0.0013)$
-20.457	$(0.125 \pm 0.0012)$
-14.436	$(0.129 \pm 0.0023)$

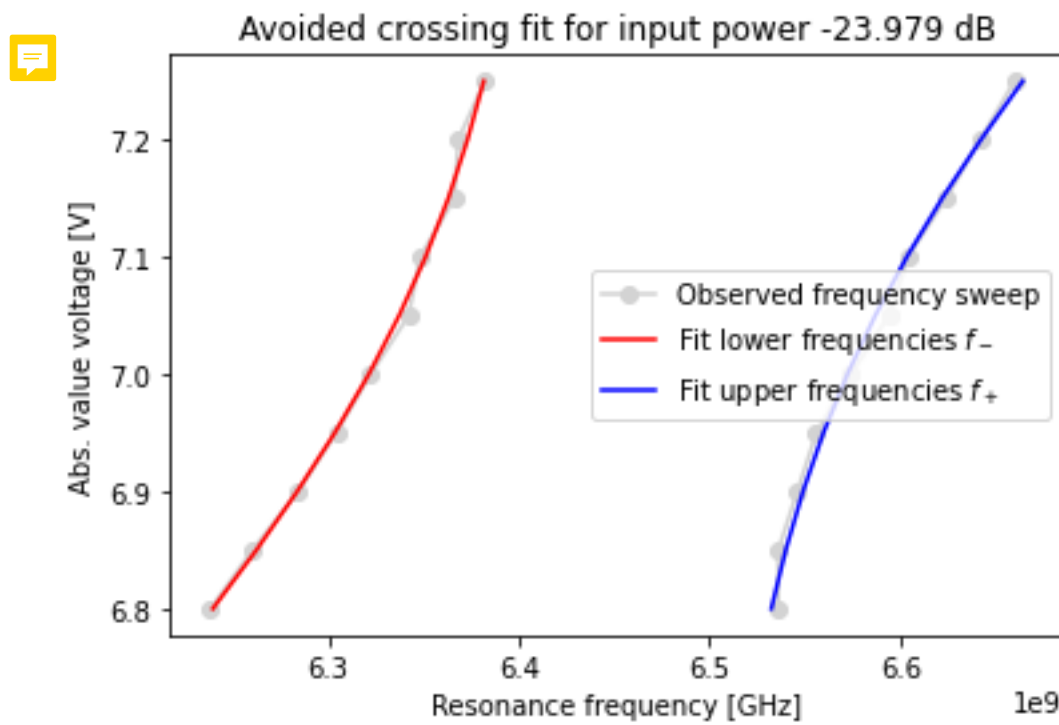


Figure 15: Graph of the fitted frequencies and the observations for an input power  $-23.979$  dB.

With these result we can again plot the relation  $g$  to input power and fit it to a third degree polynomial to see possible trends. This can be seen in fig. 16.

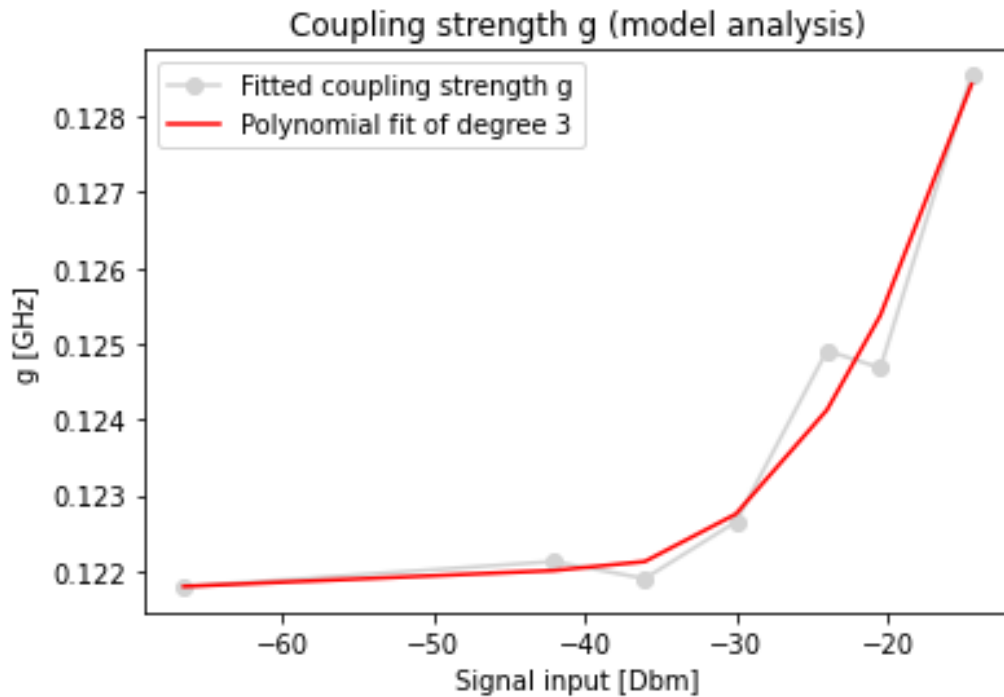



Figure 16: Plotted relation of table 4. A polynomial fit of degree 3 is also included to show a possible causal relation of input power to  $g$ .

### Interpretation of the results



In both the graphical and mathematical analysis we have obtained estimates for  $g$ . From figures 14 and 16 we see however, that the coupling strength changes with input power. Indeed, there seems to be a positive relation between signal strength and coupling strength. 



## 4 Conclusion

The experiment circuit QED has been an extraordinary **chances** to investigate quantum coupling. However, various aspects of the experiment remain elusive. What, for example are the **"noises"** at the beginning of each cavity sweep?

**It is evident that the used model needs to be adjusted and expanded.**

 Also, in order to investigate the positive relation of input power to  $g$ , it is necessary to increase the power further and observe the behaviour. Especially the phenomenon of a saturated qubit (see section 3.1.3) may be explained with the dependency of  $g$  on the input power. 

# Appendices

## A Appendix A

	Classic Mechanical	Classic Electronic	Quantum Mechanical	Quantum Electronic
Displacement	$x$	$\Phi$	$\hat{x}$	$\hat{\Phi}$
Flow	$p$	$Q$	$\hat{p} = -i\hbar \frac{d}{dx}$	$\hat{Q} = -i\hbar \frac{d}{d\Phi}$
Force	$m$	$C$	$m$	$C$
Proportionality				
Restoring	$k$	$\frac{1}{L}$	$k$	$\frac{1}{L}$
Proportionality				
Resonant Frequency	$\omega = \sqrt{\frac{k}{m}}$	$\omega = \frac{1}{\sqrt{LC}}$	$\omega = \sqrt{\frac{k}{m}}$	$\omega = \frac{1}{\sqrt{LC}}$
Commutation Relations	-	-	$[\hat{x}, \hat{p}] = i\hbar$	$[\hat{\Phi}, \hat{Q}] = i\hbar$

Figure 17: Relation between classical and electric harmonic oscillator in both the quantum and classical form.[5]

## B Appendix B

### B.1 Shortest distance

```
import numpy as np

### Find shortest distance

cut_off = 45 ### Determine cutoff from center to avoid noise

def shortest_dist(mod_mat, freq_start, freq_end, freq_steps, volt_start,
                  volt_end, volt_steps, good_start, good_end):

    nr_of_volt_measurements = np.arange(volt_start, volt_end, volt_steps).size
```

```

max_first_slice = max(mod_mat[0])

pos_max_first = np.where(mod_mat[0] == max_first_slice)[0][0]

freq_max_first = np.linspace(6.2e9, 6.8e9, 301)[pos_max_first]

distances = []

pairs = []

for i in range(good_start, nr_of_volt_measurements - good_end):

    max_global = max(mod_mat[i])

    pos_max_global = np.where(mod_mat[i] == max_global)[0][0]

    freq_max_global = np.linspace(6.2e9, 6.8e9, 301)[pos_max_global]

    max_right = mod_mat[i][pos_max_first + 20:301].max()

    pos_max_right = np.where(mod_mat[i] == max_right)[0][0]

    freq_max_right = np.linspace(6.2e9, 6.8e9, 301)[pos_max_right]

    max_left = mod_mat[i][0:(pos_max_first - cut_off)].max()

    pos_max_left = np.where(mod_mat[i] == max_left)[0][0]

    freq_max_left = np.linspace(6.2e9, 6.8e9, 301)[pos_max_left]

    pos_max1 = np.where(mod_mat[i] == max_left)[0][0]
    pos_max2 = np.where(mod_mat[i] == max_right)[0][0]

```

```
pairs.append((pos_max1, pos_max2))

dist = np.abs(np.linspace(freq_start, freq_end, freq_steps)[pos_max2] -
               np.linspace(freq_start, freq_end, freq_steps)[pos_max1]) / 10**9

distances.append(dist)

shortest_dist = min(distances)

pos_shortest_dist = distances.index(shortest_dist)

points = [pos_max1, pos_max2]

g = 0.5 * distances[pos_shortest_dist]

return pairs, g
```

## B.2 Avoided crossing

```
def avoided_crossing_direct_coupling(flux, f_center1, f_center2,
                                     c1, c2, g):
    """
    Calculates the frequencies of an avoided crossing for the following model.
    [f_1, g ]
    [g, f_2]

    f1 = c1*flux + f_center1
    f2 = c2*flux + f_center2
```

*flux: is the array of voltages*

*Data that you want to fit is the array (len(voltages, 2)) of frequencies corres*

*g: the coupling strength*

*"""*

```
frequencies = np.zeros([len(flux), 2])
```

```
for kk, dac in enumerate(flux):
```

```
    f_1 = dac * c1 + f_center1
```

```
    f_2 = dac * c2 + f_center2
```

```
    matrix = [[f_1, g],
```

```
              [g, f_2]]
```

```
    frequencies[kk, :] = np.linalg.eigvalsh(matrix)[:2]
```

```
return frequencies
```

## References

- [1] A. Blais et al. “Circuit quantum electrodynamics”. In: *Reviews of modern physics* 93 (2021).
- [2] J.M. Fink et al. “Climbing the Jaynes-Cummings ladder and observing its nonlinearity in a cavity QED”. In: *Nature* 454 (2008), pp. 315–318.
- [3] Stephanie Miller. “A tunable 20 GHz transmon qubit in a 3D cavity”. In: *ETH Zurich Semester thesis* (2018).
- [4] Andrej Tokmakoff. *Two-Level Systems*. URL: [https://chem.libretexts.org/Bookshelves/Physical\\_and\\_Theoretical\\_Chemistry\\_Textbook\\_Maps/Time\\_Dependent\\_Quantum\\_Mechanics\\_and\\_Spectroscopy\\_\(Tokmakoff\)/02%3A\\_Introduction\\_to\\_Time-Dependent\\_Quantum\\_Mechanics/2.03%3A\\_Two-Level\\_Systems](https://chem.libretexts.org/Bookshelves/Physical_and_Theoretical_Chemistry_Textbook_Maps/Time_Dependent_Quantum_Mechanics_and_Spectroscopy_(Tokmakoff)/02%3A_Introduction_to_Time-Dependent_Quantum_Mechanics/2.03%3A_Two-Level_Systems). (accessed: 12.11.2021).
- [5] Theo Walter. *Quantum Information Theory Notes*. URL: <https://qudev.phys.ethz.ch/static/content/QSIT14/QSITNotes.pdf>. (accessed: 3.11.2021).